Radiation Physics and Chemistry 188 (2021) 109683

Contents lists available at ScienceDirect

Radiation Physics and Chemistry

journal homepage: www.elsevier.com/locate/radphyschem

# Quantitative analysis of xQuant reconstruction algorithm in SPECT/CT

Ew-Jun Chen [a,b,*], Haniff Shazwan Safwan Selvam [a], Teik Hin Tan [a,b], Ming Tsuey Chew [b]

[a] Nuclear Medicine Centre, Sunway Medical Centre, No. 5, Jalan Lagoon Selatan, Bandar Sunway, 47500, Petaling Jaya, Selangor, Malaysia
[b] Centre for Applied Physics and Radiation Technologies, School of Engineering and Technology, Sunway University, No 5, Jalan Universiti, Bandar Sunway, 47500, Petaling Jaya, Selangor, Malaysia

ARTICLE INFO

*Keywords:*
xQuant
SPECT/CT
OSCGM
Quantitative
Reconstruction

ABSTRACT

Standard iterative Ordered Subset Expectation Maximisation (OSEM) reconstruction is well established in SPECT/CT, but despite its wide applications in image processing it comes with limitations in image noise and quality. A novel algorithm, xQuant (developed by Siemens Healthcare), uses Ordered Subset Conjugate Gradient Maximisation (OSCGM) which enables image quantification assessment such as standardised uptake value (SUV) measurements for reliable disease detection and evaluation of therapy response. As such, xQuant allows for dosimetry measurements, staging and management of diseases, analogous to the PET/CT modality for staging cancers and chemotherapy management. This study compares the accuracy of xQuant algorithm and current OSEM, by analysing image noise, SUV quantification and varying image reconstruction parameters. Standard clinical phantoms are used for comparison of both reconstruction algorithms: xQuant SUV accuracy with various Tc99m activity and varying scan times are performed for analysis. Results indicate that SUV measurements from xQuant are similar to expected SUV, regardless of selected reconstruction parameters, varying radiation activity and delayed scan times. Image noise assessment has shown that xQuant has lesser value of coefficient of variation (CoV) compared to standard OSEM, indicating xQuant's superior noise suppression without compromising image quality. The quantifiable superiority of xQuant reconstruction algorithm supersedes the basic iterative 3D OSEM reconstruction. It shows higher resolution qualitative assessment and provides consistent quantitative analysis. The reliability and superiority of xQuant enables clinical SPECT/CT quantification to detect disease and improve therapy management.

## 1. Introduction

The development of Single-Photon Emission Computed Tomography/Computed Tomography (SPECT/CT) has been through significant evolution, since the invention of the first gamma camera in 1958 (Hutton, 2014). The hybrid imaging modality of SPECT/CT involves multiple gamma cameras for tomographic gamma scintigraphy, combined with diagnostic CT for anatomical localisation, ultimately allowing for optimum clinical imaging. Quantitative methods have been increasingly important in recent years as technology in data acquisition and image reconstruction advances. Since radioisotopes have been introduced for diagnostic and theranostic use, accurate qualitative visualisation and true quantification of radioisotope biodistribution has been the holy grail in nuclear medicine.

The cornerstones of accurate clinical imaging are image acquisition and reconstruction, where innovative progress of both factors allows for better diagnostic confidence. OSEM is an iterative algorithm that has been traditionally used as a standard imaging reconstruction method on account of its reliability due to its good reconstruction quality and ideal convergence rate (Aijing et al., 2018). It is based on a previous reconstruction method for tomographic gamma ray imaging, Maximum Likelihood Expectation-Maximisation (MLEM), which divides the projection data into a definitive number of subsets and accesses each individually for iterative calculation (Aijing et al., 2018). Despite being widely used, traditional iterative OSEM reconstruction is well known for excessive image noise and reduced image resolution, hence it does not go through much iterations and post-filtered to control image noise (Ahn et al., 2015; Castro et al., 2018; Rahman et al., 2020).

A reconstruction algorithm developed by Siemens Healthcare, xQuant, uses a variant of iterative reconstruction named OSCGM that allows for higher resolution reconstructed SPECT/CT images and ultimately the ability to quantify them (Armstrong and Hoffmann, 2016). It uses a preconditioned ordered-subset conjugate gradient minimisation of the Mighell modified $\chi 2$ objective function, with noise and

* Corresponding author. Nuclear Medicine Centre, Sunway Medical Centre, No. 5, Jalan Lagoon Selatan, Bandar Sunway, 47500, Petaling Jaya, Selangor, Malaysia.
*E-mail address:* chenej@sunway.com.my (E.-J. Chen).

https://doi.org/10.1016/j.radphyschem.2021.109683
Received 21 April 2021; Received in revised form 23 June 2021; Accepted 25 June 2021
Available online 26 June 2021
0969-806X/© 2021 Elsevier Ltd. All rights reserved.

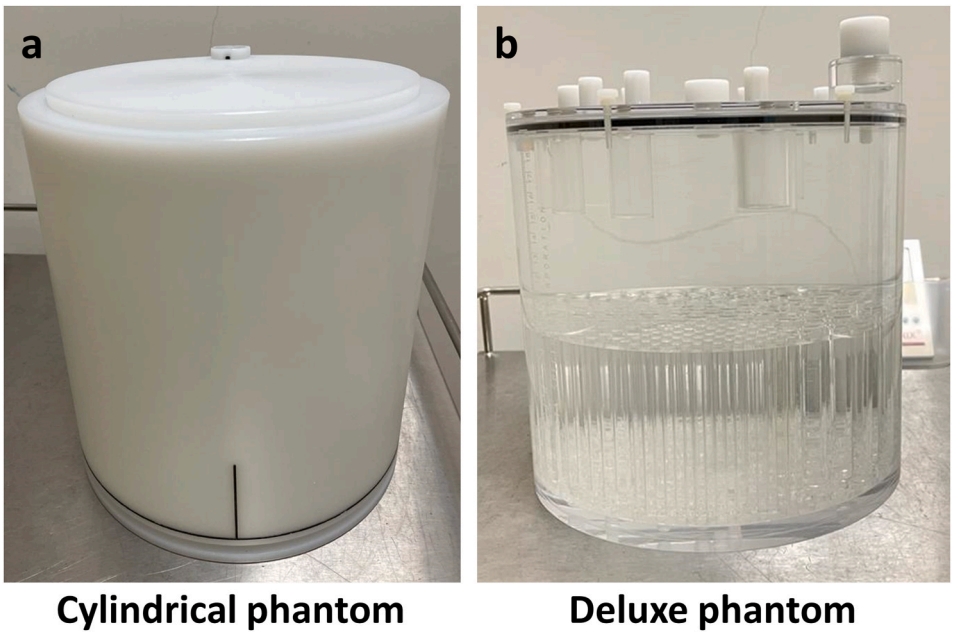


**Fig. 1.** Standard clinical phantoms used.

convergence properties different from the commonly applied OSEM (Tran-Gia and Lassmann, 2019).

Initially a construct for positron emission tomography/computed tomography (PET/CT) imaging, SUV is now a common quantitative assessment tool across nuclear medicine imaging (Dickson et al., 2019), in which it attempts to reduce observer bias and removes variability. The use of SUV as quantifiable measurement of relative tissue radioisotope uptake facilitates comparisons between patients (Kinahan and Fletcher, 2010). However, previous SPECT/CT technology has always been regarded as non-quantitative as it did not allow for SUV measurement, due to images being grossly compromised by artifacts from photon scatter and attenuation (Ritt and Kuwert, 2013; Bailey and Willowson, 2013). Healthcare companies are now providing algorithm to address this issue, such as xQuant.

This study compares the accuracy of the novel xQuant reconstruction algorithm against the current standard OSEM, with analysis of SUV accuracy, image noise, and differences in SUV by varying iterations and subsets for image post-processing and reconstruction, as discussed in methodology.

## 2. Methodology

### 2.1. Phantom preparation and image acquisition

Standard clinical cylindrical (Fig. 1a) and Jaszczak Flangeless Deluxe (Fig. 1b) phantoms were used for this study. The cylindrical phantom (Fig. 1a) is a water-filled plastic shell phantom that was provided by the manufacturer (Siemens Healthcare). It has a 20 cm inner diameter and axial length, 21 cm outer diameter, with 6283 mL volume. The Jaszczak Flangeless Deluxe phantom (Fig. 1b) provides consistent performance information for image analysis in any PET/CT or high-resolution SPECT/CT modality. Details of the Jaszczak Flangeless Deluxe are listed as below:

- Cylinder Interior Dimensions: 20.4 cm × 18.6 cm
- Volume: 6400 mL
- Cold Rod Insert Height: 8.8 cm
- Cold Rod Diameters: 4.8, 6.4, 7.9, 9.5, 11.1 and 12.7 mm
- Solid Sphere Diameters: 9.5, 12.7, 15.9, 19.1, 25.4 and 31.8 mm

**Table 1**
Examination acquisition protocol.

| Matrix size | 256*256 |
|---|---|
| Radioisotope | Tc-99m |
| Zoom | 1.00 |
| Uniformity Correction | Yes |
| Time Per View | 7 s |
| Degree of Rotation | 180 |
| Number of views | 60 |
| Mode | Continuous |
| Orbit | Non-Circular |

Both phantoms were filled with 1110 MBq of Tc-99m mixed in tap water. Phantoms were then shaken and gently rolled for 10 minutes to achieve complete homogeneity. All radiation safety precautions were strictly adhered throughout the study.

All images were acquired using Symbia Intevo 16 SPECT/CT (Siemens Healthcare). Both phantoms are scanned across multiple timepoints to achieve varying radiation dose based on decay factor calculations. Clinical scanning parameters were used and kept consistent to avoid variability for all scanning procedures, listed below in Table 1. Repetitive scanning sessions across multiple timepoints were performed to allow for analysis of SUV accuracy over change in time, by measuring against the decay of prescribed (calculated) radiation activity (i.e., 1110, 925, 740, 555 and 370 MBq). By applying various reconstruction parameters (iterations and subsets) that ultimately contribute to image quality, SUV accuracy is also analysed to determine the presence of any discrepancies.

### 2.2. Image reconstruction and analysis

After SPECT/CT acquisition, region of interest (ROI) analysis was made in the same chosen representative sections of both phantoms for all calculations to maintain consistency throughout all measurements to avoid potential discrepancies. Aforementioned sections include the top, middle and bottom axial slices of the phantoms (excluding simulated lesion areas in the Jaszczak Flangeless Deluxe phantom), with each axial slices having the mean of 5 ROIs calculated. Analysis was performed using commercially available imaging analysis software that allows for 3D volume fusion and image quantification (Syngo.Via, Siemens

| Activity (MBq) | Expected SUV | Observed SUV | Differences (%) |
|---|---|---|---|
| 1110 | 1 | 1.073333333 | 6.8 |
| 925 | 1 | 1.063333333 | 6.0 |
| 740 | 1 | 1.076666667 | 7.1 |
| 555 | 1 | 1.043333333 | 4.2 |
| 370 | 1 | 1.056666667 | 5.4 |

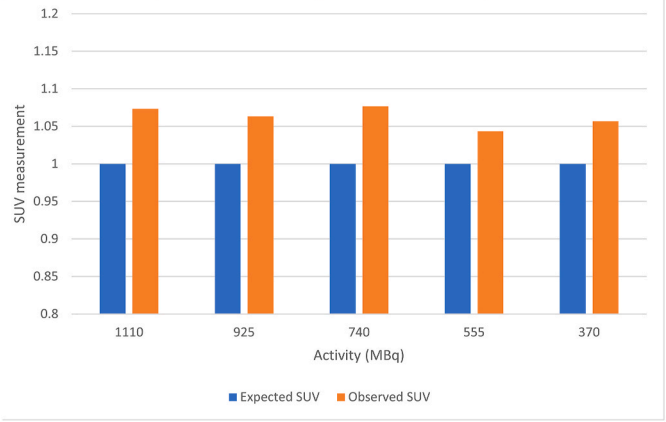


**Fig. 2.** Expected and observed SUV indicates very small (<10%) differences in xQuant SUV measurement in the cylindrical phantom.

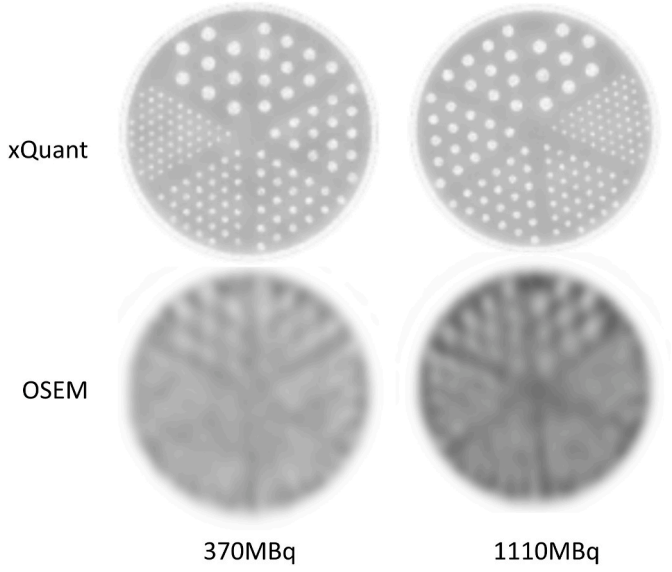


**Fig. 3.** Qualitative analysis using the deluxe phantom demonstrates superiority of xQuant (top row) over OSEM (bottom row) in image noise and resolution.

Healthcare). Analysis is divided into 3 segments:

A) Accuracy of xQuant's SUV measurement using standard clinical acquisition parameters. In this segment, 5 exact ROIs were drawn in the axial slices of phantom images, as mentioned above. Theoretical SUV is calculated and compared against observed SUV using the standardised SUV equation (Nakahara et al., 2017):

$$SUV = \frac{Activity\ concentration\ \left(\frac{MBq}{ml}\right)}{\frac{Injected\ Dose\ (MBq)}{Phantom\ Weight\ (g)}}$$

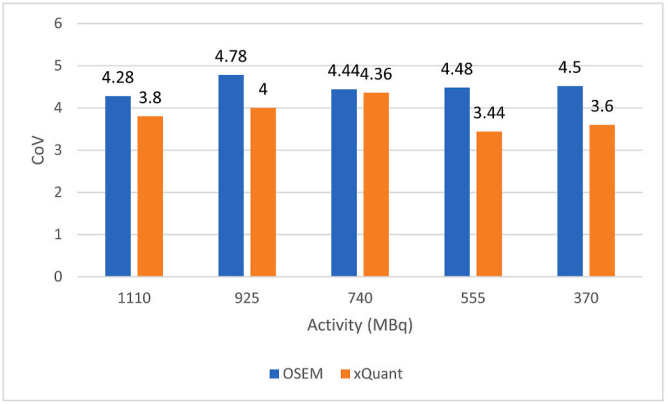


**Fig. 4.** Using the cylindrical phantom, comparison between xQuant and OSEM indicates that xQuant has a lower CoV value across all radioactivity range, therefore less noise.

B) Image noise quantification over activity decay and multiple scan times are compared between xQuant and standard OSEM. By using the same VOI drawn as above, coefficient of variation (CoV) was calculated as direct representation of image noise. This was done by taking the average of standard deviation of count over the mean count signal in all five VOIs.

C) Varying reconstruction parameters affecting accuracy of SUV. Different values of iterations (i) and subsets (s) were used in image reconstruction, ranging from standard clinical use to high values to simulate extreme trade-off between image resolution and noise (4i x 4s; 8i x 4s; 16i x 4s; 20i x 1s; 32i x 2s). Same VOI method in segment A is also repeated for SUV measurement to observe consistency of SUV accuracy from activity decay over time.

## 3. Results

For segment A of image analysis, xQuant SUV analysis revealed insignificant changes, indicative of proper clinical accuracy (Fig. 2). Based on observed SUV, there is a <10% deviation from calculated SUV, which is well within acceptable range for clinical use.

While image noise is often measured by observer biased qualitatively, it is also measured using CoV for quantitative assessment. Segment B of qualitative image analysis reveals that xQuant is more superior in both image resolution and noise reduction, at the highest (1110 MBq) and lowest (370 MBq) radioactivity (Fig. 3). Finer details in the deluxe phantom were seen more clearly in both ends of radioactivity.

CoV analysis further demonstrates superiority of xQuant over OSEM as quantitative noise assessment of xQuant is lesser than OSEM (Fig. 4). CoV is a statistical measure of the dispersion of data points in a data series around the mean, which represents the ratio of the standard deviation to the mean, thereby being a useful statistic for comparing the degree of variation from one data series to another (Tran-Gia and Lassmann, 2019; Tulik et al., 2020). Hence, as mentioned above, CoV is the representative value of image noise, with a lower CoV value indicative of less image noise.

**Table 2**
Varying reconstruction parameters shown to not affect SUV quantification across multiple radioactivity using the cylindrical phantom.

| Iteration × subset | 1110 MBq | 740 MBq | 370 MBq |
|---|---|---|---|
| 4 × 4 | 1.09 | 1.06 | 1.06 |
| 8 × 4 | 1.07 | 1.05 | 1.04 |
| 16 × 4 | 1.10 | 1.05 | 1.04 |
| 32 × 2 | 1.08 | 1.07 | 1.07 |
| 20 × 1 (xQuant) | 1.07 | 1.06 | 1.06 |


**Fig. 5.** Higher resolution in xQuant shows a tiny focal tracer uptake (arrow) which could be overlooked when compared to standard OSEM.

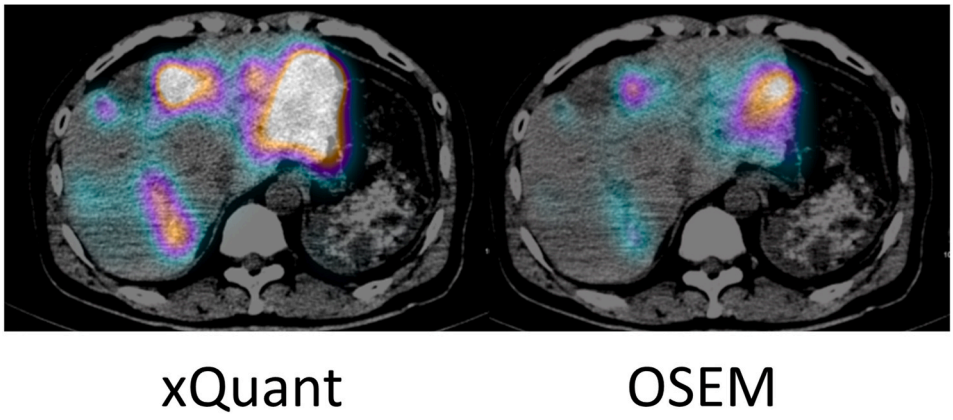


**Fig. 6.** SPECT/CT 3D volume fusion of Lutetium-177 targeted therapy demonstrates higher sensitivity and accuracy in xQuant reconstructed image (left) when compared with standard OSEM (right). Furthermore, xQuant provides SUV measurements, allowing for more accurate dosimetry treatments in patients.

The reconstruction parameters of iterations and subsets can be altered, to achieve balance between image quality and noise reduction in image reconstruction. In segment C, a range of commonly used iterations and subsets in clinical settings are applied to determine if xQuant SUV values were affected. Results indicate that SUV analysis did not deviate across all ranges of radioactivity, regardless of reconstruction parameters (Table 2). With the ranges shown in Table 2, 20i x 1s is the recommended parameter for xQuant reconstruction, as provided by engineers from Siemens, which provides an ideal trade-off between resolution and noise.

## 4. Discussion & conclusion

The consistent and reproducible quantitative analysis of SUV can increase inter-observer agreement in evaluating degree of radioisotope uptake in nuclear medicine scans (Toriihara et al., 2018). We compared and evaluated the accuracy of novel xQuant with standard OSEM in SPECT/CT image reconstruction using data from both standard clinical phantoms (cylindrical and deluxe) based on clinical acquisition protocol. Our results show that xQuant is superior to OSEM as it has increased sensitivity, better image resolution, image noise reduction and SUV quantitative accuracy as shown in Fig. 5.

SUV is the most widely used imaging quantification parameter used in clinical PET/CT examinations. Although there have been several studies reporting the use of SUV quantification in SPECT/CT studies, most describe its use in bone scintigraphy (Duncan and Ingold, 2018; Kaneta et al., 2016; Suh et al., 2016; Wang et al., 2018; Chen et al., 2021). However, SUV may also have important roles in improving accuracy and establishing quantification in SPECT/CT theranostic procedures including radioiodine, Lutetium-177 and Yttrium-90 dosimetry treatments (Fig. 6). Here, we establish the reproducibility and accuracy of xQuant as a quantifiable measurement in SPECT/CT examinations aside from bone scintigraphy. Recent studies using clinical phantoms have also supported the reproducibility of this commercially available xQuant reconstruction algorithm for reliable SPECT/CT image quantification, comparable of that to PET/CT imaging (Okuda et al., 2021; Miyaji et al., 2020).

Our study demonstrates that xQuant supersedes standard OSEM algorithm for image reconstruction, by delivering higher image resolution and lesser noise (Fig. 5). It also provides accurate and reproducible SUV measurements, similar to that of PET/CT. This quantifiable aspect of SPECT/CT is also applicable in theranostics dosimetry as it is able to measure organ specific biodistribution of radioisotopes.

## Declaration of competing interest

The authors declare that they have no known competing financial interests or personal relationships that could have appeared to influence the work reported in this paper.

## Acknowledgement

We would like to thank the Nuclear Medicine team at Sunway Medical Centre for their support and assistance.

## References

Ahn, S., Ross, S.G., Asma, E., Miao, J., Jin, X., Cheng, L., Wollenweber, S.D., Manjeshwar, R.M., 2015. Quantitative comparison of OSEM and penalized likelihood image reconstruction using relative difference penalties for clinical PET. Phys. Med. Biol. 60, 5733–5751.

Aijing, H., Xianguo, T., Rui, S., Honglong, Z., 2018. An improved OSEM iterative reconstruction algorithm for transmission tomographic gamma scanning. Appl. Radiat. Isot. 142, 51–55.

Armstrong, I.S., Hoffmann, S.A., 2016. Activity concentration measurements using a conjugate gradient (Siemens xSPECT) reconstruction algorithm in SPECT/CT. Nucl. Med. Commun. 37, 1212–1217.

Bailey, D.L., Willowson, K.P., 2013. An evidence-based review of quantitative SPECT imaging and potential clinical applications. J. Nucl. Med. 54, 83–89.

Castro, P., Huerga, C., Chamorro, P., Garayoa, J., Roch, M., Perez, L., 2018. Characterization and simulation of noise in PET images reconstructed with OSEM:

development of a method for the generation of synthetic images. Rev. Española Med. Nucl. Imagen Mol. 37, 229–236.
Chen, E.-J., Tan, T.H., Chew, M.T., 2021. Superscan: superiority of xSPECT/CT over OSEM SPECT/CT in bone scans of prostate cancer patients. Radiat. Phys. Chem. 178, 108998.
Dickson, J., Ross, J., Voo, S., 2019. Quantitative SPECT: the time is now. EJNMMI Phys. 6, 4.
Duncan, I., Ingold, N., 2018. The clinical value of xSPECT/CT Bone versus SPECT/CT. A prospective comparison of 200 scans. Eur. J. Hybrid Imag. 2, 4.
Hutton, B.F., 2014. The origins of SPECT and SPECT/CT. Eur. J. Nucl. Med. Mol. Imag. 41 (Suppl. 1), S3–S16.
Kaneta, T., Ogawa, M., Daisaki, H., Nawata, S., Yoshida, K., Inoue, T., 2016. SUV measurement of normal vertebrae using SPECT/CT with Tc-99m methylene diphosphonate. Am. J. Nucl. Med. Mol. Imag. 6, 262–268.
Kinahan, P.E., Fletcher, J.W., 2010. Positron emission tomography-computed tomography standardized uptake values in clinical practice and assessing response to therapy. Semin. Ultrasound CT MR 31, 496–505.
Miyaji, N., Miwa, K., Tokiwa, A., Ichikawa, H., Terauchi, T., Koizumi, M., Onoguchi, M., 2020. Phantom and clinical evaluation of bone SPECT/CT image reconstruction with xSPECT algorithm. EJNMMI Res. 10, 71.
Nakahara, T., Daisaki, H., Yamamoto, Y., Iimori, T., Miyagawa, K., Okamoto, T., Owaki, Y., Yada, N., Sawada, K., Tokorodani, R., 2017. Use of a digital phantom developed by QIBA for harmonizing SUVs obtained from the state-of-the-art SPECT/CT systems: a multicenter study. EJNMMI Res. 7, 1–10.
Okuda, K., Hasegawa, D., Kamiya, T., Ichikawa, H., Umeda, T., Ohkubo, T., Miwa, K., 2021. Multicenter study of quantitative SPECT imaging: reproducibility of (99m)Tc quantitation using a conjugated gradient minimization reconstruction algorithm. J. Nucl. Med. Technol. 49 (2), 138–142.
Rahman, M.A., Laforest, R., Jha, A.K., 2020. A list-mode osem-based attenuation and scatter compensation method for spect. Proc. IEEE Int. Symp. Biomed. Imag. 646–650, 2020.
Ritt, P., Kuwert, T., 2013. Quantitative SPECT/CT. Recent Results Canc. Res. 187, 313–330.
Suh, M.S., Lee, W.W., Kim, Y.K., Yun, P.Y., Kim, S.E., 2016. Maximum standardized uptake value of (99m)Tc hydroxymethylene diphosphonate SPECT/CT for the evaluation of temporomandibular joint disorder. Radiology 280, 890–896.
Toriihara, A., Daisaki, H., Yamaguchi, A., Kobayashi, M., Furukawa, S., Yoshida, K., Isogai, J., Tateishi, U., 2018. Semiquantitative analysis using standardized uptake value in (123)I-FP-CIT SPECT/CT. Clin. Imag. 52, 57–61.
Tran-Gia, J., Lassmann, M., 2019. Characterization of noise and resolution for quantitative (177)Lu SPECT/CT with xSPECT quant. J. Nucl. Med. 60, 50–59.
Tulik, M., Tulik, P., Kowalska, T., 2020. On the optimization of bone SPECT/CT in terms of image quality and radiation dose. J. Appl. Clin. Med. Phys. 21, 237–246.
Wang, R., Duan, X., Shen, C., Han, D., Ma, J., Wu, H., Xu, X., Qin, T., Fan, Q., Zhang, Z., Shi, W., Guo, Y., 2018. A retrospective study of SPECT/CT scans using SUV measurement of the normal pelvis with Tc-99m methylene diphosphonate. J. X Ray Sci. Technol. 26, 895–908.